Thermodynamics of b-HLH-LZ Protein Binding to DNA: The Energetic Importance of Protein−DNA Contacts in Site-Specific E-Box Recognition by the Complete Gene Product of the Max p21 Transcription Factor†

Laura Meier-Andrejszki,‡ Saša Bjelić,‡ Jean-François Naud,§ Pierre Lavigne,§ and Ilian Jelesarov*,‡

Biochemisches Institut der Universität Zürich, Winterthurerstrasse 190, CH-8057 Zürich, Switzerland, and Département de Pharmacologie, Institut de Pharmacologie de Sherbrooke, Université de Sherbrooke, Canada J1H 5N4

Received June 4, 2007; Revised Manuscript Received August 3, 2007

ABSTRACT: The Myc/Mad/Max network of dimeric basic region−helix−loop−helix−leucine zipper (b-HLH-LZ) transcription factors bind to enhancer box sequences (E-box) in the promotors of a large set of genes that control cell metabolism, proliferation, and differentiation. Max (Myc-associated factor X) is the obligate heterodimerization partner of Myc and Mad proteins. On the other hand, Max is the only member of the family capable of forming a stable homodimer. As part of the transcriptional regulation mechanism, Myc/Max and Mad/Max heterodimers and Max homodimers are thought to compete for binding to the E-box target sequences. E-box recognition is structurally supported by the b-HLH-LZ structural motif, which also promotes dimerization. However, the actual dimerization and heterodimerization constants of the complete gene products and their affinities for E-box sequences are not known. Also, the detailed thermodynamic characterization of DNA binding by these transcription factors has not been done yet. Such knowledge is necessary for complete understanding of the transcriptional regulation carried out by the Myc/Mad/Max network. Here, we report the first in-depth thermodynamic characterization of the stability and specific DNA binding of a full length gene product of the Myc/Mad/Max family, namely, Max protein isoform p21 (Max p21). Using calorimetric methods (DSC and ITC) we have determined the dimerization constant of Max p21 in the low micromolar range, and the Max p21/E-box complex dissociation constant in the low nanomolar range at 37 °C. The association is driven by a large exothermic effect, which is partly compensated by entropic factors. The energetic contribution to binding affinity of seven highly conserved residues that contact the DNA was probed by X-to-Ala mutagenesis. The results demonstrate that high binding affinity critically relies on the side chain of Arg 26. Furthermore, the mutational analysis points to the important role of the persistent helical turn that comprises this residue at the junction of the basic region and helix H1. Altogether, the study supports the idea that Max p21 can bind E-box sequences in vivo and likely participates directly in the regulation of transcription as homodimer.

The Max[1] protein (Myc associated factor X) belongs to the Myc/Mad/Max network of transcription factors controlling cell metabolism, proliferation, and differentiation (*1*). The network includes, next to Max, members of the Myc and Mad families, the Mad-related protein Mnt, and Mga. Max appears to have a central role in concerting the action within the network, since it is the obligate heterodimerization partner of Myc, Mad, and Mnt, thereby promoting recognition of the enhancer box (E-box) sequences in the promoters of a large set of genes, and triggering various activities of the network (*2*). Myc/Max heterodimers activate genes involved in cell growth and proliferation by the recruitment of coactivators of transcription that possess HAT activity. Myc deregulation and overexpression is associated with apoptosis, genetic instability, and malignant transformations, such as small cell lung cancer, neuroblastoma, and glioblastoma (*3*). The Mad/Max heterodimer antagonizes most of Myc/Max transcriptional activities by recruiting corepressors with HDAC activity (*4*). The Mnt/Max heterodimer also has a tumor suppressor activity (ref (*5*) and citations therein). While Myc, Mad, and Mnt proteins have short half-lives and their expression levels are strictly controlled by diverse signal transduction cascades like the MAP-kinase or TGF-β pathway, Max itself has a significantly longer half-life and is stably and ubiquitously expressed. Max is the only member of the family which is capable of forming sufficiently stable homodimers (*in vitro*). However, *in vitro* studies with truncated constructs demonstrate that the $(Max)_2$ homodimer is less stable than the Myc/Max and Mad/Max heterodimers (*6*). Being transcriptionally inert and lacking the domains

† This work was supported by the Swiss National Center of Competence in Research "Structural Biology" and in part by Grant 31-100197/1 from the Swiss National Science Foundation and the Canadian Institutes for Health Research.

* To whom correspondence should be addressed. Phone: ++41 44 635 5547. Fax: ++41 44 635 6805. E-mail: iljel@bioc.unizh.ch.

‡ Biochemisches Institut der Universität Zürich.

§ Université de Sherbrooke.

[1] Abbreviations: b-HLH-LZ; basic−helix−loop−helix−leucine zipper; DSC, differential scanning calorimetry; E-box, enhancer box; HAT, histone acetyl transferase; HDAC, histone deacetylase; ITC, isothermal titration calorimetry; Mad, mitotic absence deficient; Max, Myc-associated factor X; MRE, mean residue ellipticity; Myc, myelocytoma-associated protein; ΔG, free energy change; ΔH, enthalpy change; ΔS, entropy change; ΔC_p, heat capacity change.

10.1021/bi701081q CCC: $37.00
Published on Web 10/04/2007

necessary for recruiting coactivator or corepressor protein complexes, Max is hypothesized to be able to modulate cell growth by competing for E-box with Myc/Max, Mad/Max, or Mnt/Max. It is still unknown whether the competition proceeds at the level of heterodimer-*versus*-homodimer E-box binding affinity discrimination, or else $(Max)_2$ binding to DNA reduces the concentration of Max monomers available for heterodimerization with other family members.

All members of the Myc/Max/Mad network contain a basic region−helix−loop−helix−leucine zipper (b-HLH-LZ) structural motif, which is responsible for DNA binding and dimerization, flanked by sequences that are involved in recruiting of effector partner proteins. The crystal structures of c-Myc/Max, Mad1/Max, and $(Max)_2$ proteins bound to E-box have revealed a very similar structural organization of the b-HLH-LZ domains in the context of either homodimeric $(Max)_2$ or of the heterodimers (*7*−*9*). The HLH domain folds as a parallel four-helix bundle. A parallel, two-stranded coiled coil is formed by the adjacent LZ domains. The basic region domains form α-helices naturally emerging from the end of helix H1 of HLH and diverging to grip the duplex by fitting into the major groove. It has been long suggested that the basic region segments undergo a conformational transition from a quasi-random coil in the free protein to an α-helix in the protein−DNA complex (*10*, *11*). Very recently, the structure of the unbound $(Max)_2$ b-HLH-LZ homodimer was determined by NMR, for the first time allowing insights into the structural rearrangements accompanying DNA recognition (*12*). Indeed, the first 14 residues of the basic region are largely unfolded in the absence of DNA. Interestingly, however, the last four residues of the basic region form a highly populated helical turn, just adjacent to helix H1 of HLH. Since highly conserved basic residues contacting the E-box site are located in this region, it was plausibly suggested that prefolded α-helical conformers might speed up specific binding. The loop region possesses high flexibility in the free state. Little difference was observed in the conformation of the LZ coiled coil domain in the free and in the bound state.

Specific E-box binding by Myc/Mad/Max family members is mediated by conserved side chains from the basic region. Structural studies have identified a conserved and quasi-symmetric recognition pattern within the 5′-CACGTG-3′ target, including four specific hydrogen bonds to DNA bases and a number of nonspecific electrostatic contacts with the phosphate backbone. In addition, residues from the loop region closely approach the duplex and are seemingly involved in binding. There is some controversy about the number of protein−DNA backbone contacts: Six such interactions have been identified in the structure of the $(Max)_2$−DNA complex (*7*). While additional contacts, both from the basic region and from the loop regions, are made by the Myc protein in the Myc/Max−DNA complex (*9*), there is no structural evidence that the regions flanking the b-HLH-LZ domain are involved in E-box recognition.

Although the structural basis of E-box recognition by b-HLH-LZ proteins of the Myc/Mad/Max family is now firmly established, much less is known about the energetics of binding and the relative affinities of different dimers for the cognate DNA sequence. So far, only the binding affinity of short constructs encompassing the b-HLH-LZ core domain has been determined (*13*−*15*). In the present study we use calorimetry to characterize thermodynamically the site-specific binding of the complete Max p21 isoform to a 21 base pair DNA duplex containing the E-box sequence. By examining the thermal stability of Max p21 and Max p21/DNA complex, we provide for the first time a reliable estimate of the dissociation constant at the physiologically relevant temperature of 37 °C. X-to-Ala mutations reveal the energetic importance of specific and nonspecific protein−DNA contacts. Direct binding experiments demonstrate that stabilization of the leucine zipper domain increases the DNA-binding affinity.

EXPERIMENTAL PROCEDURES

Buffer. All biophysical experiments were performed in a standard buffer containing 100 mM sodium phosphate, pH 6.8. The buffer was supplemented with 100−600 mM KCl. The pH of samples containing urea was adjusted after addition of the denaturant. The urea concentration was determined by measuring the refractive index. All chemicals were of analytical grade and were used without further purification.

Molecular Biology, Protein Expression, and Purification. The construction of the pET3a expression plasmid and expression of Max p21, Max p21VL, and Max_{SS} has been described (*16*, *17*). Site directed mutagenesis was carried out using commercially available kits from QIAGEN following the protocol recommended by the manufacturer. The primers designed for mutagenesis PCR are available on request. After expression, the cells were frozen and stored at −20 °C. Purification was done as described before (*16*, *17*). In an additional purification step, the combined fractions after ion exchange chromatography were dialyzed against water overnight, loaded on a semipreparative C8-HPLC column, and eluted with binary acetonitrile/water gradients (3% to 60%) containing 0.1% and 0.085% trifluoroacetic acid. The material after HPLC was lyophilized. The protein refolded from the lyophilized state was fully native, as judged by CD spectroscopy, and displayed DNA binding affinity indistinguishable from that measured with natively purified non-lyophilized material. The purity was verified by analytical HPLC with detection at 220 nm, and the mass was verified by mass spectrometry. The concentration was measured by UV spectroscopy using $\epsilon_{280} = 5960\ M^{-1}\ cm^{-1}$ calculated from the amino acid sequence.

DNA Synthesis and Annealing. The 21 bp DNA single strand oligonucletides bearing the E-box target site (see Figure 1) were custom-synthesized (Metabion GmbH). After HPLC purification, they were dissolved in water and the concentration was determined by UV after complete digestion with phosphodiesterase overnight at 37 °C. The annealing was done by mixing equimolar amounts of both strands in 100 mM potassium chloride. The sample was incubated at 90 °C for 5 min and then slowly cooled down over 4 h. Concentration of the double stranded E-box was determined by UV spectroscopy after digestion with phosphodiesterase, and the annealing was confirmed by agarose gel electrophoresis.

Circular Dichroism (CD) Spectroscopy. Circular dichroism spectroscopy was perfomed on a Jasco J-715 spectropolarimeter equipped with a computer-controlled water thermostat using jacketed quartz cells of 0.2, 0.5, or 1 cm optical path

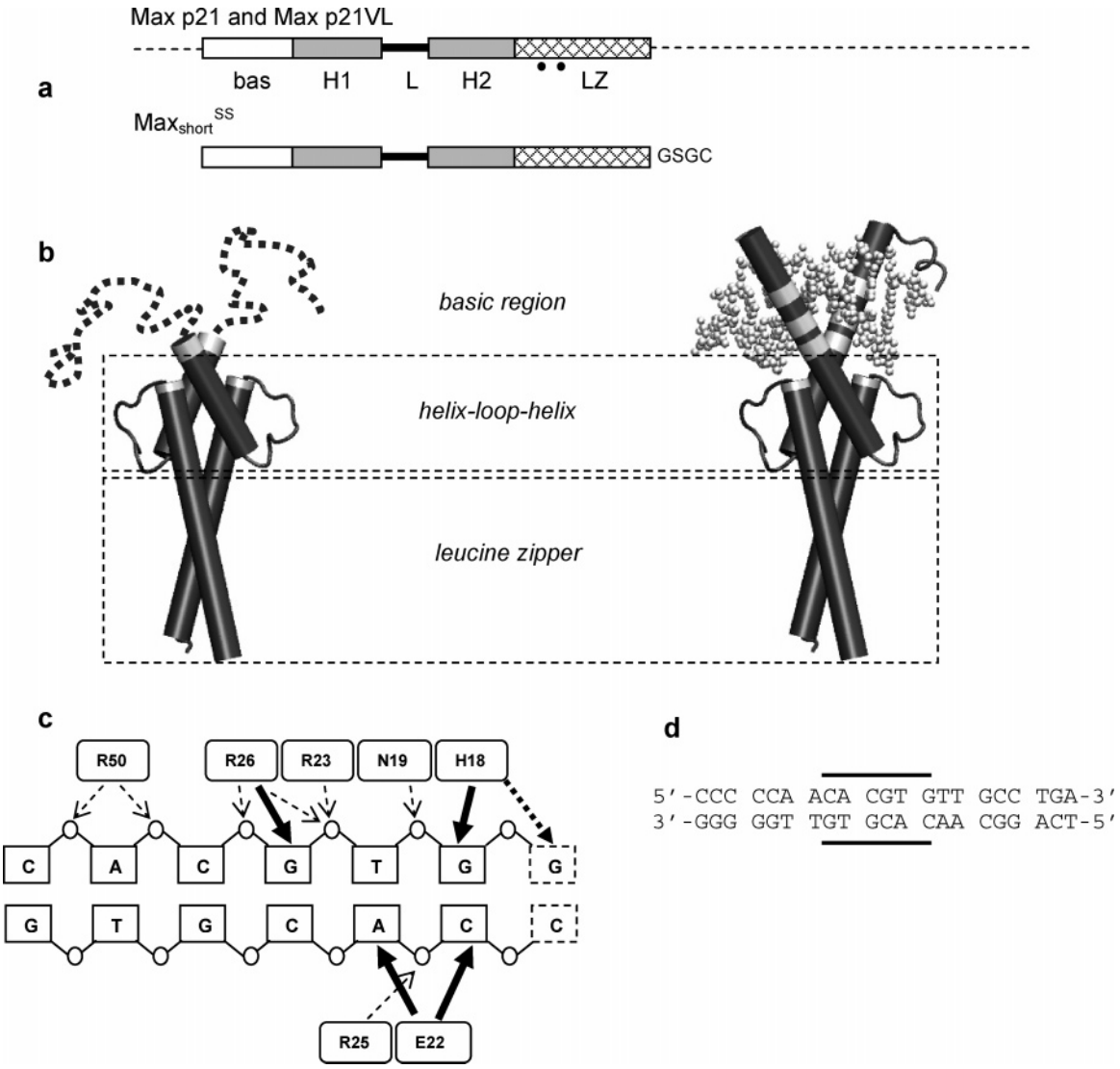

FIGURE 1: Structure of Max p21 and protein−DNA interactions in the Max p21-E-box complex. (a) Sequential organization. White bar, basic region (bas). Gray bars, α-helices (H1 and H2). Hatched bar, leucine zipper (LZ). Thick line, loop (L). The dashed lines are the unstructured N- and C-terminal segments. The length of the schematic elements is proportional to the corresponding sequence length. The positions of the N69V and H72L mutations in Max p21VL are indicated with dots. In the lower scheme, the structure of the short constructs is shown. Max_{short} lacks the unstructured segments outside the b-HLH-LZ core domain. The GSGC C-terminal extension facilitates formation of the disulfide linked Max_{short}^{SS} protein. (b) E-box binding does not perturb the structure of HLH and LZ, but the basic region folds from a predominantly coil conformation to a regular α-helix fitting into the DNA major groove. In the cartoon representation residues contacting DNA are shown in white. Note that the very C-terminus of the basic region containing the DNA-contacting Arg 25 and Arg 26 is part of an α-helical turn also in the free protein. (c) Protein−DNA interactions within the E-box target sequence. The protein−DNA contacts formed by one of the protein monomers are shown as bold arrows (base-specific hydrogen bonds) and thin arrows (contacts to the phosphate backbone. (d) Sequence of the DNA duplex used in this study. The E-box is demarcated.

length. Spectra were recorded at a scanning speed of 5 nm min^{-1} and 0.2 nm intervals. Three scans were averaged to obtain the final spectrum. Isothermal urea unfolding experiments were performed at 5, 20, and 25 °C. The samples were incubated overnight and the ellipticity at 222 nm was sampled for 3 min after thermal equilibration. The data were analyzed following the linear extrapolation model (LEM) as detailed elsewhere (*18*). The concentration dependence of ellipticity at 222 nm was studied with 1−100 μM (monomer equivalents) protein solutions. Thermal denaturation was performed by monitoring the change in ellipticiy at 222 nm during continuous heating at 1 deg min^{-1} between 5 and 75−90 °C. Reversibility was checked from the recovery of the CD signal after cooling, and was at least 90% in all cases.

Isothermal Titration Calorimetry. ITC experiments were performed on a VP-ITC instrument (MicroCal Inc., Northampton, MA). The calorimeter was calibrated according to the manufacturer's instruction. Samples of protein and DNA were prepared in, and thoroughly dialyzed against, the same batch of buffer to minimize artifacts due to minor differences in buffer composition. The concentration was determined after dialysis. The sample cell (1.4 mL) was loaded with 8−20 μM (dimer equivalents) protein; DNA duplex concentration in the syringe was 90−300 μM. A titration experiment typically consisted of 25−30 injections, each of 8 or 10 μL volume and 10 or 12 s duration, with a 5 min interval between additions. Stirring rate was 300 rpm. Raw data were integrated, corrected for nonspecific heats, normalized for concentration, and analyzed according to a 1:1 binding model assuming a single set of identical binding sites.

Differental Scanning Calorimetry. DSC experiments were performed on a VP-DSC calorimeter (MicroCal Inc.) equipped

with twin coin-shaped cells of 0.52 mL volume. Details on the instrument's performance are given elsewhere (*19*). The heating rate was 1 °C min^{-1}. Samples containing protein and DNA (in isolation or as a mixture) were dialyzed for 18−24 h against the same batch of buffer used to establish the instrumental buffer−buffer baseline. Reversibility was checked by 2−3 cycles of heating and cooling. The raw experimental data were corrected for the instrumental baseline and transformed to partial molar or partial specific heat capacity using partial specific volumes calculated from the amino acid composition. The analysis of heat capacity traces followed the formalism detailed elsewhere (*20*, *21*). Data handling and analysis were carried out using the program CpCalc 2.1 (Applied Thermodynamics), subroutines for Origin provided by MicroCal, and in-house written scripts for NLREG (Phillip H. Sherrod).

RESULTS AND DISCUSSION

A schematic representation of the structural organization of the full gene product of the Max p21 protein and its b-HLH-LZ domain (henceforth referred to as Max p21 and Max_{short}, respectively) is shown in Figure 1. The figure indicates also the position of the cysteine residue which was introduced at the C-terminus of the leucine zipper to produce the disulfide-linked variant Max_{short}^{SS} after oxidation, as well as the location of the N68V and H71L mutations in the Max p21VL variant. All proteins were expressed in soluble form in the cytoplasm of *Escherichia coli*. Purified Max p21 exists as a homodimer in the concentration range 15 to 120 μM (monomer equivalents) under the experimental conditions used in this study, as evidenced by equilibrium and velocity analytical ultracentrifugation (see Figure S1 in Supporting Information).[2] We first describe spectroscopic characterization and unfolding experiments aimed at determination of the thermodynamic stability of Max p21. This information is important in order to carry out the binding experiments in the temperature range where Max p21 is in its fully native and dimeric state. ITC and DSC experiments revealing the energetics of Max p21 binding to E-box DNA are presented in the second part. In the third part, we evaluate the energetic role of conserved Max p21 side chains to the DNA binding affinity from binding experiments with Max p21 variants, in which particular protein−DNA contacts were removed by mutation to alanine.

Stability and Unfolding Energetics of Max p21

The N- and C-Terminal Extensions of the Max b-HLH-LZ Domain Are Disordered. The CD spectrum of Max_{short} is typical for a protein with high helical content (Figure 2, trace b). The per-residue molar ellipticity (MRE) of Max p21 is significantly lower (trace a). However if one expresses the CD signal of Max p21 normalized for 86 residues (the length of Max_{short}), instead of 150 residues (the length of Max p21), one can appreciate the spectroscopic signature of the N- and C-terminal segments that are not present in Max_{short} (trace c). The normalized MRE_{222} of Max p21 (trace c) is slightly more negative (indicating higher helical content) than MRE_{222} of Max_{short} (trace b). The difference is likely due to the fact that the fraction of unfolded (monomeric and nonhelical) Max_{short} is 5−10% at the selected concentration (100 μM; ref (*17*)), whereas Max p21 is more than 98% dimeric (20 μM; see Figure 5). In contrast, the decrease in ellipticity below 210 nm is pronounced and is accompanied by a blue shift as expected for the existence of unfolded segments. It follows that the ∼70 "extra" residues beyond the b-HLH-LZ core domain of Max p21 are apparently devoid of stable secondary structure elements.

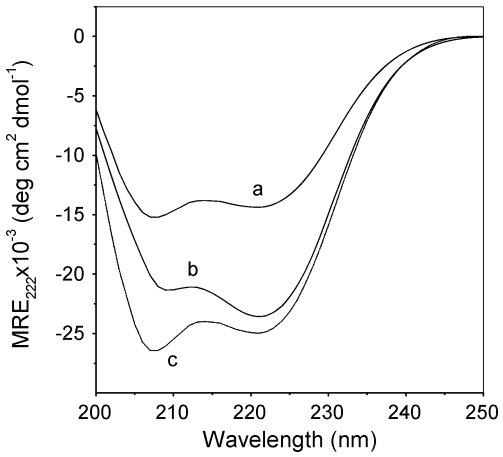

FIGURE 2: Far-UV CD spectra of Max p21 (trace a) and Max_{short} (trace b) at 25 °C in standard buffer. Concentrations were 20 μM Max p21 and 100 μM Max_{short} (monomer equivalents). Trace c represents MRE_{222} of Max p21 recalculated for 86 amino acid residues per monomer (see the text for details).

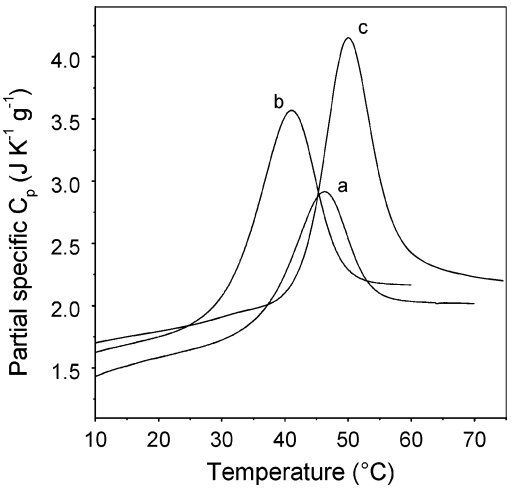

FIGURE 3: Partial specific heat capacity of Max p21 (trace a), Max_{short} (trace b), and Max_{short}^{SS} (trace c). Concentrations were 125 μM Max p21, 280 μM Max_{short} (monomer equivalents), and 100 μM Max_{short}^{SS}.

The participation of unstructured polypeptide domains in intra- or intermolecular contacts cannot be excluded *a priori* on the basis of spectroscopic data. Scanning calorimetry experiments were performed to check whether the N- and C-terminal extensions of the b-HLH-LZ domain contribute to the unfolding enthalpy. Max p21 exhibits a significantly lower partial specific enthalpy than Max_{short} (Figure 3). When compared at the same temperature (43 °C, selected in between the corresponding melting temperatures to minimize the errors of extrapolation) these enthalpies amount to 10.5

[2] We have not performed AUC experiments with Max_{short} and Max_{short}^{SS}. However, the partial molar heat capacity of both proteins between 5 and 25 °C shows no concentration dependence up to ∼300 μM monomer concentration. All DSC traces are well described by a two-state unfolding model. Such behavior is a strong evidence that oligomerization does not take place.

$\pm$ 0.5 J g^{-1} (Max p21) and 17.1 $\pm$ 0.7 10. J g^{-1} (Max_{short}). The ratio is thus 0.61, close to the molar mass ratio (0.59). Furthermore, the temperature slopes of the partial specific heat capacities in the native region are very close to each other, ~13 J K^{-2} g^{-1}. Hence, within the limit of detection there are no enthalpically rich packing interactions involving molecular segments outside the core b-HLH-LZ domain. Altogether, the presented calorimetric results provide sound evidence that the N- and C-terminal domains of Max p21 are unfolded, as previously suggested on the basis of spectroscopic data only (*16*). Interestingly, the Max_{short}^{SS} variant, in which the C-terminals of the leucine zipper are linked by a disulfide bond, unfolds with a specific unfolding enthalpy of 20.1 $\pm$ 0.2 J g^{-1} (at 43 °C; see Figure 3). This observation is in accord with the suggestion that the C-terminal part of the leucine zipper is partly or completely unfolded (*16*). The disulfide link tethers the frying (or unfolded) C-termini and assists folding (coiled coiling) along the entire length of the leucine zipper, an effect manifested with heat release.

Unfolding Energetics. Although essentially unstructured and not participating in packing interactions with either each other or with the b-HLH-LZ domain, the "tails" confer significant stabilization to Max p21 (Figure 3). The molecular basis of stabilization is unclear at present, but it was hypothesized that the stabilization originates from electrostatic effects (*16*). Indeed, it was suggested that the abundance of negative charges in the N-terminal segment of Max p21 might help to overcome the electrostatic destabilization originating from charge−charge repulsion between clusters of positive charges at the HLH interface around helix H1 (*12*). At the melting temperature of 46.3 °C (125 μM monomer concentration) the calorimetric estimates of the unfolding parameters are $\Delta H_{cal} = 370 \pm 20$ kJ mol^{-1}, $\Delta S_{cal} = 1.1 \pm 0.1$ kJ K^{-1} mol^{-1}, and $\Delta C_p = 3.6 \pm 0.4$ kJ K^{-1} mol^{-1}. Using the temperature of maximal heat absorption (T_{max}), the molar heat capacity at that temperature ($C_{p,max}$), the unfolding heat capacity increment (ΔC_p), and the (assumed) molecularity of unfolding process ($n = 2$), the effective van't Hoff enthalpy can be calculated as $\Delta H_{vH} = (\sqrt{2} + 1)T_{max}\sqrt{R(C_{p,max} - (\Delta C_p\sqrt{n})/(\sqrt{n+1}))} = 400$ kJ mol^{-1}. Thus, the ratio $\Delta H_{vH}/\Delta H_{cal}$ is 1.07, in reasonable agreement with a two-state unfolding between folded dimer and unfolded monomer. The highly cooperative character of unfolding is further supported by the coincidence the unfolding parameters derived by calorimetry (this study) and thermal melting followed by CD spectroscopy (*16*).

Stability Curve of Max p21. The stability of Max p21 at 5, 20, and 25 °C was assessed from isothermal urea-induced unfolding experiments by following the change in ellipticity at 222 nm. The data could be modeled with a two-state transition between native and unfolded protein (Figure 4). As shown in Figure 5, the agreement between ΔG_U values thus obtained and data obtained from DSC experiments is excellent. At 37 °C, the dissociation constant is $K_D = 3.6 \times 10^{-6}$ M and compares well with the only one previous estimate of 7.1×10^{-6} M (*16*). For the isolated b-HLH-LZ domain K_D at 37 °C was 100×10^{-6} M, obtained from CD thermal melting (*17*). Fluorescence anisotropy assay yielded a K_D ~0.7×10^{-6} M at 20 °C (*13*). For comparison, our estimate for the stability of Max p21 at 20 °C is 0.004×10^{-6} M. These results are in further support of the pronounced stabilization effect the disordered extensions exert on the core b-HLH-LZ domain.

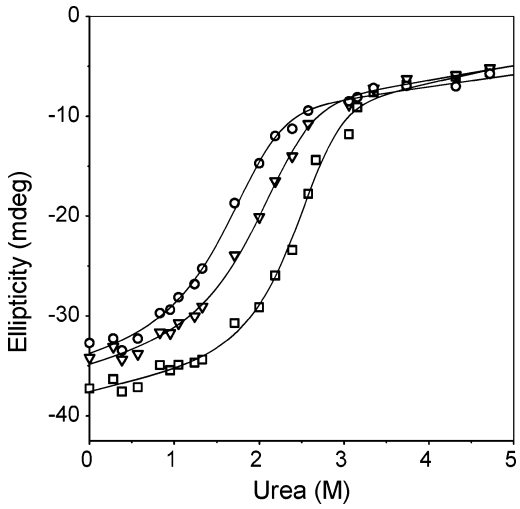

FIGURE 4: Urea-induced unfolding of Max p21. Experiments were performed with 30 μM protein (monomer equivalents) at 5 °C (squares), 20 °C (triangles), and 25 °C (circles). The solid lines are best fits according to a two-state unfolding model assuming equilibrium between folded dimer and unfolded monomer.

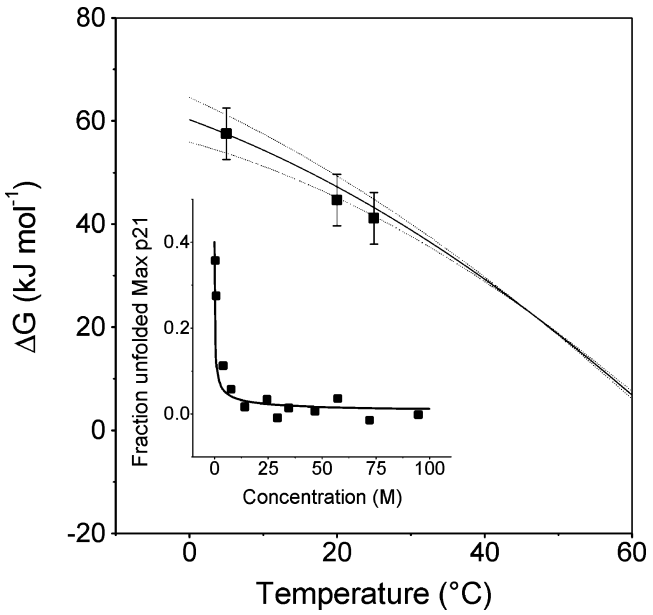

FIGURE 5: Thermodynamic stability of Max p21. The solid line represents the stability curve calculated from calorimetric data: $T_m = 46.3$ °C (125 μM monomer concentration), $\Delta H_{cal} = 370 \pm 20$ kJ mol^{-1}, and $\Delta C_p = 3.6 \pm 0.4$ kJ K^{-1} mol^{-1}. The dotted lines are the upper and lower error margins introduced by the experimental uncertainty. The symbols are ΔG measured by urea-induced denaturation at 5, 20, and 25 °C (data in Figure 4). Inset: Fraction unfolded Max p21 at 25 °C as a function of the protein concentration. The solid line is the function calculated as $f_U = (-K_D + \sqrt{K_D^2 + 8K_D M})/(4M)$, where $K_D = \exp[-\Delta G/(RT)]$ and M is the concentration in monomer equivalents. The symbols are the experimentally observed changes in ellipticity.

The stability curve (Figure 5) was used to simulate the fraction of unfolded protein as a function of the protein concentration (solid line, inset of Figure 5). The simulation was verified by measuring the change of MRE_{222} (and the fraction unfolded) as a function of the total protein concentration (symbols in the inset of Figure 5). As one can notice,

the experiment is in excellent agreement with the simulation, and demonstrates consistently that the dimeric state is populated to more than 97% for protein concentrations down to 10 μM between 5 and 25 °C. Hence, binding experiments were designed in this temperature and protein concentration range. Finally, the stability of Max p21 is insensitive to mutations in the basic region. Indeed, the midpoints of thermal denaturation measured by CD spectroscopy for all 7 variants studied here were within ±1 degree (not shown).

Thermodynamics of DNA Binding by Max p21

Experimental Design. Protein−DNA binding experiments are typically performed by titrating protein into DNA solution placed in the calorimetric cell. In cases of high affinity binding, low reagent concentrations are required to collect data allowing reliable calculation of the association constant and the binding enthalpy from the same binding isotherm (*22*). If the protein placed in the injection syringe is composed of noncovalently associated subunits, care should be taken that the protein concentration after dilution in the cell is always high enough, so that no dissociation takes place. Unfortunately, the thermodynamic stability of Max p21 is relatively low and a significant shift of the monomer−dimer equilibrium occurs at subsaturating concentrations (0.1−5 μM; see Figure 5). In contrast, the stability of the 21 bp DNA duplex used in this study is very high. From DSC data (duplex unfolding enthalpy was 570 kJ mol^{-1} at 80° for melting of 17 μM duplex), the duplex dissociation constant is on the order of 10^{-19} M and, therefore, no strand dissociation takes place down to low sub-micromolar concentrations. For this reason the ITC titrations were performed by titrating E-box duplex DNA into Max p21. To verify that the choice of titrant and titrand does not influence the results, control experiments of titrating protein into DNA or titrating DNA into protein were performed with the monomeric Max_{short}^{SS} protein. The results were identical within error. However, this setup does not overcome the problem that there is a redistribution of the population of dimer and monomer during the titration experiment, since the cell contents become progressively diluted, and the free Max p21 concentration decreases as the saturation of DNA binding sites increases. As justified in the Supporting Information, due to the fortuitous combination of Max p21 dissociation constant, Max p21 dissociation enthalpy, and the large enthalpy change characterizing the formation of the Max p21/DNA complex, the heat effect of the monomer−dimer transition concomitant to binding is relatively small and influences the shape of the binding isotherm only slightly. The error from neglecting the monomer−dimer redistribution is not larger than the typical error caused by the uncertainty in concentration determination and the instrumental peak repeatability. The systematic overestimation of the molar binding enthalpy is ∼6 kJ mol^{-1}, as compared to a standard deviation of 6 kJ mol^{-1} calculated from triplicate experiments performed with different protein and DNA batches. The "distorted" binding constants are within the usual error range ±10−50%. We demonstrate below that the reported binding constants from ITC are in a very good correspondence with data derived from independent experiments. While, strictly speaking, the reported thermodynamic parameters are apparent, they are nevertheless reliable. It is important to note that the binding energetic differences reported next for the discussed mutants are not affected. Indeed, all Max p21 mutant proteins exhibit the same thermodynamic stability.

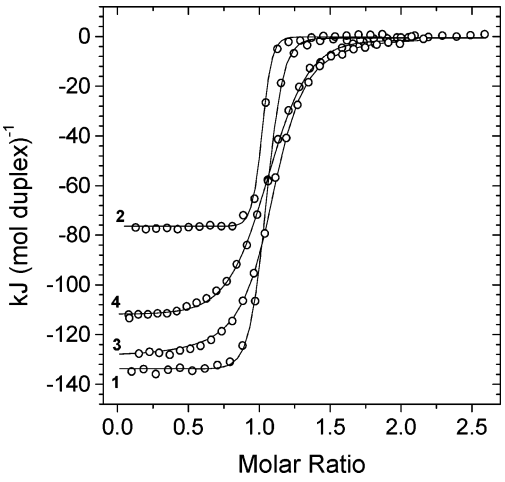

FIGURE 6: Examples of calorimetric isotherms describing binding of Max p21 to E-box DNA. The heats measured at each titration step were normalized for the molar concentration and corrected for unspecific heats (symbols). The continuous lines visualize best fits according to a 1:1 binding model. The figure illustrates the temperature variation of the binding enthalpy (compare trace 1 measured at 25 °C and trace 2 measured at 8 °C) and the decrease in affinity caused by addition of salt at 25 °C (total salt concentration was 150 mM (trace 1), 400 mM (trace 3), and 500 mM (trace 4)).

Thermodynamic Profile of the Wild Type Max p21/E-Box Complex. Examples of binding isotherms measured by ITC are shown in Figure 6. Addition of aliquots of E-box DNA duplex to Max p21 produces exothermic heat effects, which saturate as the molar ratio of duplex to Max p21 dimer increases. The stoichiometry in the data set was 0.98 ± 0.07 Max p21 dimer per DNA duplex (mean ± SD of more than 50 experiments, including experiments with Max p21 variants), in agreement with a 1:1 protein−DNA complex seen in the crystal structures of Max p21/E-box, c-Myc/Max/E-box, and Mad/Max/E-box complexes. There are suggestions that members of the Myc/Mad/Max family can form dimers of dimers via association patches provided by the leucine zipper domains (*23*). Indeed, tetrameric c-Myc/Max and Max/Max (but not Mad/Max) species binding two copies of the cognate DNA were observed by X-ray crystallography (*7*, *9*). However, ultracentrifugation experiments performed with concentrations typically used in ITC experiments at our experimental conditions failed to detect the presence of tetramers (see Figure S1 in the Supporting Information). Therefore, the measured thermodynamic parameters truly reflect the energy changes promoting formation of the Max p21 dimer to the E-box site.

Analysis of the binding isotherms obtained in standard buffer conditions and between 5 and 25 °C reveals that the association is enthalpy-driven and is opposed by entropy (Table 1). In this temperature range binding is too strong to obtain reliable estimates of the association constant, K_A, with reactant concentration in the low micromolar range. However, the binding enthalpy, ΔH_A, and its temperature dependence, $\Delta C_{p,A}$, are defined with high precision. The same ΔH_A was measured in phosphate and Tris buffers

Table 1: Thermodynamic Parameters Characterizing Max p21 and Max p21 Variants Binding to E-box DNA Measured by ITC[a]

protein	$K_A \times 10^{-7}$ (M^{-1})	ΔG_A (kJ mol^{-1})	ΔH_A (kJ mol^{-1})	$T\Delta S_A$ (kJ mol^{-1})	ΔS_A (J K^{-1} mol^{-1})	$\Delta C_{p,A}$ (kJ K^{-1} mol^{-1})
Max p21	38.00 69.00[b]	−48.9	−137	−88	−295	−3.8
Max p21VL	610.00	−55.8	−140	−84	−282	nd[c]
Max_{short}^{SS}	480.00	−55.2	−129	−74	−248	−3.8
Max $p21^{H18A}$	2.30	−42.0	−124	−82	−275	−3.8
Max $p21^{N19A}$	180.00	−52.8	−133	−80	−268	−4.2
Max $p21^{E22A}$	2.15	−41.8	−126	−84	−282	−3.6
Max $p21^{R23A}$	2.23	−41.9	−130	−88	−295	−3.6
Max $p21^{R25A}$	0.22	−36.2	−125	−89	−300	−3.3
Max $p21^{R26A}$	$<10^{-3}$	>-25.0	nd	nd	nd	nd
Max $p21^{R50A}$	0.55	−38.5	−159	−119	400	−4.1

[a] All experiments were performed at 25 °C in 100 mM Na-phosphate, 100 mM KCl, pH 6.8, unless otherwise indicated. The standard error of K_A, δK_A was maximum 60%. Thus, the maximum error of ΔG_A is $\delta\Delta G_A = RT(\delta K_A/K_A) = 1.5$ kJ mol^{-1}. The maximum error of ΔH_A, $\delta\Delta H_A$, was on the order of 6 kJ mol^{-1}. The error of $T\Delta S_A$ is $\delta T\Delta S_A = \sqrt{(\delta\Delta H_A)^2+(\delta\Delta G_A)^2} = 6.5$ kJ mol^{-1}. The error of $\Delta C_{p,A}$ was estimated as ±0.2 kJ K^{-1} mol^{-1} by jackknife tests. [b] From DSC data according to eqs 1−3. [c] Not determined.

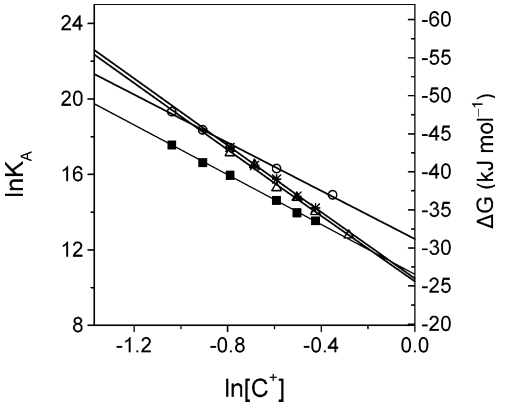

FIGURE 7: Influence of salt concentration on the affinity of Max p21 variants to E-box DNA. The binding constants were measured by ITC at 25 °C in increasing concentrations of KCl. Filled squares, wild type Max p21. Circles, Max $p21^{N19A}$. Triangles, Max_{short}^{SS}. Asterisks, Max p21VL. The lines are linear fits according to eq 4. Extrapolation to the left *y*-axis yields $K_A = e^{\ln K_A}$ at the standard buffer conditions (0.154 mM cation concentration), which are listed in Table 1. Extrapolation to the right *y*-axis yields the nonelectrostatic contribution to ΔG_A (ΔG^{ne}) estimated at 1 M cation concentration. The slopes of the straight lines equal the product $Z\psi$ as defined in eq 4.

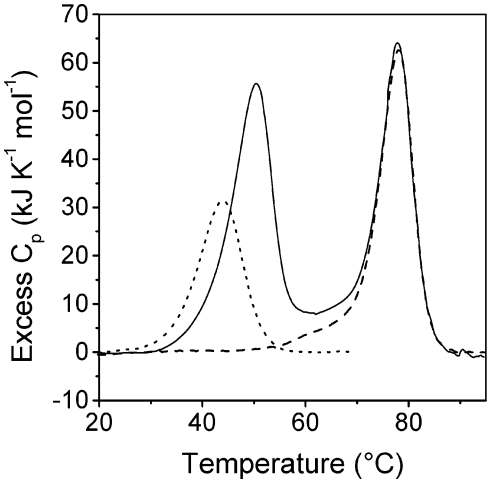

FIGURE 8: DSC melting profiles of Max p21 (dotted line), E-box DNA (dashed line), and the 1:1 protein−DNA complex (continuous line). The concentration of all species was 17 μM (protein dimer, DNA duplex, and complex).

having different heats of protonation. Hence, there is no (net) proton release/uptake accompanying binding.

In order to get an accurate estimate of K_A, we explored the well-known sensitivity of protein−DNA complexes to the concentration of cations (*24*, *25*). Binding experiments were performed in increasing concentrations of KCl at 25 °C. As illustrated in Figure 6 the binding isotherms become increasingly shallower at higher salt concentration because binding gets weaker (by a factor 55 from 350 mM to 650 mM cation concentration). Reliable K_A can be calculated from such isotherms. As in many documented cases, in the absence of specific anion effects, ln K_A depends linearly on the logarithm of cation concentration (ln [C^+]) in the range of salt concentrations where the water activity is negligibly perturbed by the presence of salt (Figure 7). Linear extrapolation to our standard buffer conditions yields $K_A(25\ °C) = (3.8 \pm 0.2) \times 10^8\ M^{-1}$ ($K_D = (2.7 \pm 0.1) \times 10^{-9}$ M).

Whereas changes of K_A with temperature, pH, and pressure have a rigorous thermodynamic basis, this is not the case for the effect of salt. To verify the reliability of the linear extrapolation, DSC experiments were designed to obtain an independent estimate of K_A. To this end, DSC melting traces were recorded with Max p21, E-box DNA duplex, and the 1:1 Max p21/E-box complex. The midpoints of thermal unfolding of Max p21 and E-box DNA are separated by ∼35 °C (Figure 8). Melting of the 1:1 complex produces two peaks. The first one overlaps partially with the thermogram of isolated Max p21 and corresponds to cooperative protein−DNA complex melting, which is intimately coupled to Max p21 unfolding. The ∼7 °C shift in the temperature of maximum heat absorption relative to the maximum of the Max p21 peak reflects the stabilization of the protein caused by protein−DNA contacts. Melting of the complex releases free DNA duplex, which melts at a much higher temperature (the second peak of the continuous trace in Figure 8). Using the known unfolding enthalpy (ΔH_P) and unfolding heat capacity change ($\Delta C_{p,P}$) of the Max p21 at the melting temperature (T_P) in the absence of DNA, the association constant K_A at the temperature corresponding to half-completion of complex melting (T_C) can be calculated according to the following equation (*26*):

$$K_A(T_C) = \frac{\exp\left\{-\frac{\Delta H_P}{R}\left(\frac{1}{T_C}-\frac{1}{T_P}\right)+\frac{\Delta C_{p,P}}{R}\left(\ln\frac{T_C}{T_P}+\frac{T_P}{T_C}-1\right)\right\}-1}{[D]_{T_C}} \quad (1)$$

The term $[D]_{T_C}$ in the denominator of eq 1 is the concentration of free DNA duplex at T_C. Since binding is strong, the population of the 1:1 complex is higher than 0.98 at the onset of heat absorption (~30 °C) and, therefore, $[D]_{T_C} = [D]_{tot}/2$. The calculated K_A(50 °C) is $(1.9 \pm 0.3) \times 10^6$ M^{-1}. This number compares well with $K_A(50\ °C) = (1.3 \pm 0.5) \times 10^6$ M^{-1} obtained by using the parameters directly measured by ITC at 25 °C according to

$$K_A(T_C) = K_A(25\ °C)\exp\left\{-\frac{\Delta H_A(25\ °C)}{R}\left(\frac{1}{T_C}-\frac{1}{298.15}\right)+\frac{\Delta C_{p,A}}{R}\left(\ln\frac{T_C}{298.15}+\frac{298.15}{T_C}-1\right)\right\} \quad (2)$$

The data from ITC (ΔH_A and $\Delta C_{p,A}$) and DSC (K_A(50 °C)) can be combined to yield an estimate of K_A at 25 °C:

$$K_A(25\ °C) = K_A(50\ °C)\exp\left\{-\frac{\Delta H_A}{R}\left(\frac{1}{298.15}-\frac{1}{323.6}\right)+\frac{\Delta C_{p,A}}{R}\left(\ln\frac{298.15}{323.6}-\frac{298.15}{323.6}+1\right)\right\} \quad (3)$$

The resulting K_A is $(6.9 \pm 2) \times 10^8$ M^{-1}, in close agreement with the value obtained by linear extrapolation of the data collected at high-salt conditions ($(3.8 \pm 0.2) \times 10^8$ M^{-1}). The consistency of the binding constants in an extended temperature interval allows a reliable estimate of the stability of the Max p21/E-box complex at 37 °C: $(4 \pm 1) \times 10^7$ M^{-1} ($K_D = (25 \pm 6) \times 10^{-9}$ M). To our knowledge, this is the first direct estimate of the binding affinity of the complete gene product of Max p21 to E-box at the physiologically relevant temperature. Previously, the affinity of the b-HLH-LZ to E-box containing DNA duplexes was estimated to be in the range 1 and 30 nM at temperatures between 20 and 37 °C and at similar buffer conditions (*13*, *14*). It follows that while the protein N-terminal and C-terminal regions outside the b-HLH-LZ contribute to the stability of the p21 dimer, they are not involved in any significant interactions with DNA.

The thermodynamic parameters describing formation of the Max p21/E-box complex at 25 °C are $\Delta G_A = -48.9 \pm 2.0$ kJ mol^{-1}, $\Delta H_A = -137 \pm 8$ kJ mol^{-1}, $\Delta S_A = -0.295 \pm 0.025$ kJ K^{-1} mol^{-1} ($T\Delta S_A = -88 \pm 8$ kJ mol^{-1}), and $\Delta C_{p,A} = -3.8 \pm 0.2$ kJ K^{-1} mol^{-1} (Table 1). Both ΔH_A and $T\Delta S_A$ are large numbers, which cannot be interpreted as the enthalpy accumulated in intermolecular bonds, or as the entropy change associated with these bonds. Rather, the total binding parameters contain the energetic expenditures for the conformational transition of the basic region from the largely unfolded, free state to its α-helical, bound state. Considering ΔH_A, the "genuine" binding enthalpy can be estimated by subtracting the enthalpy of α-helix formation from the total observed enthalpy change. Fourteen residues per Max chain undergo coil-to-helix transition (*12*). The enthalpy of helix formation was estimated as −2.5 to −3.8 kJ mol residue^{-1} depending on the chemical identity of the side chain involved (*27*), and the weight of evidence suggests −4 kJ mol residue^{-1} as the upper limit for a typical hydrogen bond (*28*). Combining these numbers, the "genuine" enthalpy stabilizing the Max p21/E-box complex can be estimated as −25 to −40 kJ mol^{-1}. Assuming that formation of 10 hydrogen bonds, as seen in the crystal structure, represents the major enthalpic contribution to binding, the mean enthalpic content of such bonds is −2.5 to −4.0 kJ mol^{-1}, in agreement with the estimated enthalpic content of hydrogen bonding cited just above. A very similar picture was recently suggested for DNA recognition by the b-ZIP domain of GCN4, on the basis of direct measurement of the enthalpic contribution for folding of the similarly long basic region (*29*). The large unfavorable entropy change indicates that the loss of conformational entropy dominates the entropic benefits from dehydration of molecular surface and the polyelectrolyte effect. According to a back-on-the-envelope calculation the sum of the entropic contributions (in J K^{-1} mol^{-1}) arising from (i) immobilization of 22 side chains becoming buried by ≥20 Å^2 in the complex (−300; ref (*30*)), (ii) immobilization of the backbone of 28 residues (−420; ref (*31*)), (iii) dehydration of molecular surface (+310, considering only the protein−DNA interface dehydration; (*32*)), (iv) polyelectrolyte effect (+120; ref (*25*)), and (v) loss of translational and rotational degree of freedom (−35: ref (*33*)) predicts a total predicted entropy change of −325 J K^{-1} mol^{-1}, as compared to the experimental value of −295 J K^{-1} mol^{-1}. The calculation is indeed very crude, yet it might give some idea about the balance of entropic factors involved in complex formation. From the reduction of solvent accessible surface, one can estimate that the dehydration of the protein−DNA interface will cause a heat capacity decrease of approximately 0.4 J K^{-1} mol^{-1}, ten times lower than the experimental value (−3.8 J K^{-1} mol^{-1}). However, Dragan et al. convincingly demonstrated that the similar discrepancy observed for GCN4 b-ZIP binding to DNA is caused by the temperature-induced changes in the structural content (and the extent of DNA-induced refolding for that matter) of the basic region in the temperature range of ITC experiments (*29*). In principle, the effect can be quantified by comparing the temperature dependence of the heat capacities measured for the associated and dissociated state of the protein−DNA complex (*34*, *35*). Unfortunately, the limited solubility of Max p21 precluded precise heat capacity measurements in sufficiently concentrated solutions. Nevertheless, the sum of the heat capacities of the isolated components is significantly higher than the heat capacity of the Max p21/DNA complex and the difference strongly depends on the temperature. As explained in detail in the Supporting Information, from the available data we estimate that the temperature-induced shift of the coil-to-helix equilibrium of the basic region and any other temperature-dependent structural changes collectively contribute ~−3 kJ mol^{-1} K^{-1} to the apparent ΔC_p. Hence, ΔC_p arising from intermolecular interactions and dehydration of the surface is ~−1 kJ mol^{-1} K^{-1}, or even smaller (see above).

Number of Cations Released upon Binding and Electrostatic Contribution to ΔG_A. The linear dependence between $\ln K_A$ and $\ln [C^+]$ allows estimation of the number of cations

released from the phosphate backbone upon protein binding, i.e., the number of protein−phosphate backbone ionic contacts (*24*, *25*). Furthermore, the electrostatic and nonelectrostatic components of the total binding free energy can be estimated (*29*). For the equilibrium process

$$P + D + nC^+ \rightleftarrows PD + mC^+$$

the following equation holds (*25*):

$$\ln K_A = \ln K_A^{ne} - Z\psi \ln [C^+] \quad (4)$$

P, D, and PD represent the equilibrium concentrations of protein, DNA, and protein−DNA complex, respectively; C^+ is the molar concentration of cations; n and m are the stoichiometric coefficients. $Z = (n - m)$ represents the number of protein−DNA ionic contacts, and $\psi = 0.64$ is the number of released cations per phosphate group (*36*). From the slope of the plot according to eq 4, $Z = 10.3$. Therefore, the estimated number of ionic contacts bridging Max p21 to the E-box phosphate backbone is 5 per Max p21 chain. Crystallographic analysis identified the existence of 6 such contacts (*7*). Given the quality of the experimental data, the discrepancy is unlikely caused by experimental uncertainties. Rather, we presume that one of the suggested contacts is not realized in solution at the selected conditions. Incidentally, the same sensitivity on the cation concentration as the wild type complex was observed for the Max $p21^{N19A}$ mutant ($Z = 9.9$; see Figure 7). Since Asn 19 is one of the side chains implicated in electrostatic interaction with the phosphate backbone, it appears plausible to assume that the contact seen in the X-ray structure is not populated in solution. Interestingly, the closest distance of Asn 19 (via OD1) to the DNA backbone is larger than 3.8 Å in the structure of the Max b-HLH-LZ/DNA complex (1AN2; (*8*)). In fact, the replacement of the Asn19 side chain by alanine stabilizes the complex (see below), which is difficult to comprehend if favorable polar interactions with DNA occur at that site. The conclusion is supported by analysis of the total binding free energy in terms of electrostatic and nonelectrostatic components. The nonelectrostatic component of ΔG_A can be roughly estimated from $-RT \ln K_A$ according to eq 4 in the limit of $[C^+] = 1$ M, since the second term of eq 1 is zero. Although it is not possible to estimate to what extent electrostatic effects are attenuated at this salt concentration, it appears that they contribute almost half of the binding free energy measured for Max p21 binding at 25 °C ($\Delta G^{el} \sim -22$ kJ mol^{-1}; see Table 1 and Figure 7). The electrostatic contribution to ΔG_A of the Max $p12^{N19A}$/DNA complex is identical within error with that of the wild type complex, indicating that the affinity increase caused by the N19A mutation is governed by nonelectrostatic effects (ΔG^{nel}, Table 2).

Stabilization of the Leucine Zipper Domain Increases the DNA-Binding Affinity of Max p21. The Origin of the Phenomenon Is Electrostatic. Spectroscopic data have shown that the midpoint of thermal dissociation of the Max b-HLH-LZ/DNA complex is shifted to higher temperature if LZ of Max is stabilized (*16*). However, the origin of this effect has never been pursued in detail. Now we provide hints about the molecular origin of the phenomenon. As seen in Table 1, either introduction of an S−S bridge at the C-terminus of the leucine zipper of the core b-HLH-LZ domain, or the double N68V/H71L mutation in the context of the full length Max p21 increases K_A by a factor of 12−15. Both variants are significantly more stable than the wild type counterparts (*16*, *17*) (see also Figure 3 to compare the stability of Max p21 and Max_{short}^{SS}). From the data taken at face value from Table 1 it would appear that stabilization of the leucine zipper favors binding entropically, especially when the chains of b-HLH-LZ are covalently linked in the Max_{short}^{SS} variant. Still, the observed decrease in ΔH_A off-setting the entropic benefit is not easy to understand. In Max p21VL better binding is accomplished by simultaneous action of enthalpic and entropic factors, yet the enthalpy−entropy balance remains elusive, since the differences are clearly within the experimental error margins. There are reasons to hypothesize that DNA contacts from the loop region and/or helix H1 are created or become stronger in the stabilized versions of Max b-HLH-LZ. Indeed, the more stable complexes formed by Max p21VL and Max_{short}^{SS} are also more sensitive to the concentration of cations. Formation of both complexes is accompanied by the release of 7 cations per binding site ($Z = 13.8$ for Max p21VL and $Z = 13.7$ for Max_{short}^{SS}; see Table 2 and Figure 7). It follows that some additional electrostatic contacts in these variants increase the DNA-binding affinity and these new contacts are restricted to side chains within the b-HLH-LZ domain. It turns out that ΔG^{el} is significantly larger in the case of Max p21VL and Max_{short}^{SS} binding ($\Delta G^{el} \sim -30$ kJ mol^{-1}). In fact, the observed increase in ΔG^{el} completely explains the stronger binding of Max p21VL and Max_{short}^{SS}, since the nonelectrostatic component of ΔG_A, $\Delta G^{nel} = \Delta G_A - \Delta G^{el}$, is identical within error for Max p21, Max p21VL, and Max_{short}^{SS}.

Table 2: Number of Cations Released upon Formation of the Max p21/DNA Complex and Estimation of the Electrostatic and Nonelectrostatic Contribution to ΔG[a]

protein	Z[b]	ΔG^{nel} [c]	ΔG^{el} [d]	ΔG^{nel} [d]
Max p21	10.3 ± 0.1	-48.9 ± 0.2	-22.4 ± 0.3	-26.5 ± 0.2
Max p21VL	13.8 ± 0.1	-55.8 ± 0.2	-29.9 ± 0.3	-25.9 ± 0.2
Max_{short}^{SS}	13.7 ± 0.1	-55.2 ± 0.2	-29.7 ± 0.3	-25.5 ± 0.2
Max $p21^{N19A}$	9.9 ± 0.1	-52.8 ± 0.2	-21.6 ± 0.3	-31.2 ± 0.2

[a] At 25 °C, pH 6.8, ΔG values in kJ mol^{-1}. [b] Calculated as $Z = -\mathrm{d} \ln K_A/\mathrm{d}[C^+]/0.64$. [c] Nonelectrostatic contribution to ΔG_A estimated from $-RT \ln K_A$ at 1 M cation concentration. [d] Electrostatic contribution to ΔG_A estimated from $\Delta G^{el} = \Delta G_A - \Delta G^{nel}$.

Altogether, the data strongly suggest that the Asn 19 side chain is not involved in electrostatic contacts with the DNA backbone, while additional protein−phosphate backbone interactions are responsible for the higher-affinity binding of the variants with stabilized b-HLH-LZ domain. We are reluctant to embark on lengthy speculations as to which side chains may be involved. In principle, there are many highly conserved basic residues in close proximity to the DNA backbone, involving the presumably quite unrestrained stretch Lys 13-Arg 14-Arg 15 preceding the "canonical" portion of the basic region (His 18 to Arg 26), Lys 24 in the middle of the basic region, Lys 30 from helix H1, as well as Lys 47 from the loop region. Indeed, some of these interactions were described in or can be surmised from the crystal structures of the c-Myc-Max−E-box and $(Max)_2$−E-box complexes, both containing only the b-HLH-LZ

protein domains (*8*, *9*). The feasibility of these contacts is less obvious in the only available structure of the Max p21/E-box complex. It is perhaps most natural to assume that a more stable, and possibly less fluctuating leucine zipper alters the structural or dynamic properties, or both, of the adjacent HLH domain. It has been argued that stabilization of structural scaffolds or stabilization of local conformations could improve the DNA-binding affinity of transcription factors (*37*, *38*). Possibly, conformational rearrangement of the loop region and slight positional reorientation of helices H1 and H2 facilitate new protein−DNA contacts. In fact, the NMR structure of the free, disulfide linked Max b-HLH-LZ domain bearing the N68V/H71L double mutation indicates a loop conformation facilitating direct contact of Lys 47 and Ser 49 to DNA phosphates (*12*). Lys 47 points away from the duplex in $(Max)_2$/E-box X-ray structure. As another, very likely candidate we suggest Lys 30 of helix H1, which forms very well-defined charge−charge contacts with DNA phosphates (distance <3.5 Å) in both monomers of the c-Myc-Max/E-box complex.

Mutational Analysis of the Max p21/E-Box Interface

On the basis of structural information six residues from the highly conserved basic region of the Max p21 monomer contact the Cyt(1)-Ade(2)-Cyt(3)-Gua(4)-Thy(5)-Gua(6) E-box core sequence (*7*). (Although more contacts could be inferred from the X-ray structures of $(Max)_2$/E-box, c-Myc-Max/E-box and Mad-Max/E-box complexes formed by the corresponding b-HLH-LZ core domains, we analyze the contacts as they are defined in the only available complex of the full length Max p21.) Residues His 18, Glu 22, and Arg 26 are involved in specific hydrogen bonds to DNA bases. Mutation of Glu 22 abolishes discrimination between E-box and nonspecific DNA (*39*). The contact formed by Arg 26 to the central guanine crucially governs the specificity of b-HLH-LZ proteins for class B E-box elements (*40*). Arg 26 is anchored also to the DNA backbone since both NH2 and Nϵ atoms are positioned very close to phosphate oxygen atoms. Nonspecific interactions with the phosphate backbone are formed by Asn 19, Arg 23, and Arg 25. Arg 50, which is located at the start of helix H2, makes a main-chain and a side-chain contact with backbone phosphates. A schematic representation of the interactions is shown in Figure 1. To probe for the energetic role of particular contacts we replaced the corresponding side chains by alanine and determined the energetic signature of the mutant complexes by ITC. The measured thermodynamic parameters at 25 °C are listed in Table 1.

Figure 9 illustrates the changes in the energetic profile of the mutant Max p21/E-box complexes. The bars represent $\Delta\Delta G$, $\Delta\Delta H$, and $T\Delta\Delta S$ values ($\Delta\Delta X = \Delta X^{mutant} - \Delta X^{wild\ type}$) calculated for binding of the Max p21 dimer to E-box duplex. We would like to remind the reader that the indicated energetic differences are the combined effect of two simultaneous mutations, one on each monomer. We assume that the structural symmetry seen in the crystal structure translates into energetic equality of the contacts realized in the two half sites. Removal of the base-specific hydrogen bond of Arg 26 by replacing the central E-box guanine by cytosine in one or both E-box half sites has demonstrated essentially no cooperativity (*6*). This result should not be taken as ultimately proving the independence of the half sites since all other protein−DNA contacts have been left intact in the cited study. Small distance differences between interacting groups might result in serious energetic differences. However, we are not aware of any study documenting cooperativity between half sites in DNA recognition by (structurally) symmetrical homodimer proteins.

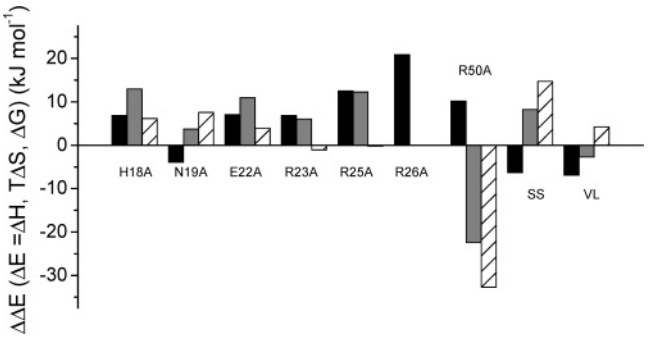

FIGURE 9: Changes in the energetic profile of the Max p21/E-box complex upon alanine substitution or LZ stabilization. The bars represent the changes in ΔG_A (black), ΔH_A (gray), and $T\Delta S_A$ (hatched) calculated as $\Delta\Delta E = \Delta E^{mutant} - \Delta E^{wildtype}$ (numerical ΔE values from Table 1). $\Delta\Delta G > 0$ indicates that the mutation is destabilizing. Mutations are destabilizing the complex enthalpically if $\Delta\Delta H > 0$. Entropically favorable mutations are manifested by $T\Delta\Delta S > 0$. All experiments were performed at 25 °C in the standard buffer.

Three mutations, H18A, E22A, and R23A, exhibit modest decreases of affinity (∼sixteen time increase in K_D). The effect of removal of Arg 25 and Arg 50 is more pronounced (a K_D increase of 160 and 60 times, respectively). Two mutations stand out. The wild type Asn 19 side chain appears to destabilize the complex relative to alanine. Removal of the Arg 26 side chain beyond the C_β atom is extremely destabilizing. We cannot give a very precise estimate for the decreased affinity of the Max $p21^{R26A}$ protein. ITC experiments were not possible at concentrations sufficiently high as to allow precise measurement of the binding constant at 25 °C. The observed heat effect of binding was small as well. These experiments indicated ∼50 μM as the lower bound of K_D. Since the pronounced reduction of heat release relative to wild type binding introduced ambiguity in the ITC results, another estimate of the Max $p21^{R26A}$ affinity was obtained by CD spectroscopy. Recently, it was convincingly demonstrated that the decrease in MRE_{222} upon titration of Max p21 with increasing amounts of DNA directly reflects the population of the protein/DNA complex (*41*). Mixing of equimolar (50 μM) Max $p21^{R26A}$ and E-box duplex results in a decrease in MRE_{222} of 400 deg cm $dmol^{-1}$. This is ∼15% of the average MRE_{222} decrease observed at full saturation (3000 deg cm $dmol^{-1}$). With this information, K_D ∼200 μM was calculated. Irrespective of the exact K_D value, it is clear that the R26A mutation destabilizes the complex by a factor of at least 10^4 (K_D).

Is it possible to rationalize the energetic effect of the mutations? Visual inspection of the protein/DNA cocrystal structure provides clues for some sites. Removal of the four base-specific and buried hydrogen bonds formed by Glu 22 to N4 of Cyt(1) and N6 of Ade(2) (two hydrogen bonds per half site) is energetically not very costly: each bond contributes 1.7 kJ mol^{-1} on average to ΔG_A. Interestingly, if the bonds are broken by mutating out the hydrogen donors, the average contribution per hydrogen bond is more than

twice larger, 3.7 kJ mol^{-1} (*41*). It is likely that the carboxyl group of Glu 22 experiences large unfavorable dehydration, which is uncompensated in the absence of hydrogen bond partners. The problem appears relieved in the Max $p21^{E22A}$ mutant lacking the side chain carboxylate. The dramatic destabilization caused by the Arg 26 replacement is surprising at first glance, since the contribution of each base-specific hydrogen bond between NH1 of Arg 26 and N7 of Gua(4) has been recently estimated as 2−3 kJ mol^{-1} (*6*). It should be noted, however, that the Arg 26 side chain is engaged additionally in two sugar−phosphate backbone contacts, which are also lost (broken) in the R26A mutant studied here. Apart from the energetic contribution of each sugar−phosphate backbone contact *per se* (which can be substantial as seen in Figure 9) such interactions might help to fix the arginine side chain in a position for optimal hydrogen bonding and certainly help to overcome the entropic loss from freezing of the side chain. In any case, Arg 26 represents a crucial "hot spot" at the binding interface.

Overall, there is a large variation in the destabilizing effect of the mutations. On average, backbone contacts contribute more to stabilization of the complex than base-specific hydrogen bonds. This is in line with previous studies with X-to-Ala mutations showing that substitution of residues making contacts with the sugar−phosphate backbone may produce mutant proteins more severely defective in DNA binding than substitution of residues making base-specific contacts (e.g., (*42*)). The energetic content of such "unspecific" interactions might also differ considerably. A clear example is presented by Arg 23 and Arg 25, the effect of the latter being twice larger. In fact, Arg 23 is oriented much more favorably toward the phosphate oxygen atoms than Arg 25. However, it is also significantly more exposed to the solvent than Arg 25. Moreover, we note that the Arg 25 Nϵ atom faces the carboxylic group of Glu 22 (it is <3.5 Å away from both carboxylate oxygens). This observation suggests that the Arg 25 side chain may help in optimizing the geometry of the base-specific contacts of Glu 22. If so, it exerts an "indirect" additional stabilization of the complex, which is lost upon mutation to alanine. Particularly intriguing is the role of Asn 19. The residue is highly conserved within the Myc/Max/Mad network of transcriptional factors and it closely approaches the DNA backbone according to structural data, yet the removal of this contact by mutating out the asparagine amide group increases the affinity for DNA. According to the original annotation of the available coordinate files the contact to the phosphate oxygen is made by either OD1 or ND2 atoms of Asn 19 (distance <3 Å). Since the assignment of the electron density to OD1 or ND2 atoms in not very highly resolved structures is ambiguous, we have attempted a simple visual evaluation of the possibility that the potentially unfavorable Asn OD1-to-O1P contact can be relieved by rotating the $C_\beta-C_\gamma$ bond to position ND2 close to O1P. No clear conclusions could be drawn. It appears that the environment of the Asn 19 amide group is electrostatically intensive due to the close proximity of groups bearing partial positive charge (ND1 of His 18) or partial negative charge (the carbonyl oxygen of Arg 15) and bound water molecule(s). We are currently investigating the problem by means of MD simulations.

Concerning the energetic partitioning of the changes in affinity, we cannot provide a detailed structural explanation of the observed enthalpy−entropy balance of particular mutations. First, the experimental error is sizable in comparison to the magnitude of the measured $\Delta\Delta H_A$ and $\Delta\Delta S_A$. Second and more important, binding is tightly coupled to (partial) coil-to-helix transition of the Max p21 basic region and to bending of the E-box duplex. In principle, the energetic signature of these processes could be affected by mutation. Third, replacement of larger side chains having polar groups by small and nonpolar alanine could have caused redistribution of water molecules at and near the binding interface. With these considerations in mind, in the following we briefly discuss some general trends and possible sources of the energetic signature of some mutations.

We first consider mutations in the basic region, excluding the R26A mutation, for which $\Delta\Delta H_A$ and $\Delta\Delta S_A$ could not be measured. The R50A replacement, which is outside the boundaries of the basic region, exhibits a completely different energetic signature and should be discussed separately. It is clear from Figure 9 that all mutations in the basic region are linked to loss of enthalpic interactions, including the stabilizing N19A replacement. For side chains stabilizing the protein−DNA complex, the magnitude of enthalpic destabilization upon mutation dominates over the entropic effect, but there is no correlation between the total destabilization ($\Delta\Delta G$) and its enthalpic ($\Delta\Delta H$) and entropic ($\Delta\Delta S$) components, as noted in diverse other macromolecular systems. Removal of a backbone contact could be enthalpically as costly as the removal of two hydrogen bonds (R25A *versus* H18A and E22A). The enthalpic contribution from formally identical backbone contacts could also be very different (R23A *versus* R25A). In fact, the enthalpy term completely determines the magnitude of stabilization provided by the latter two arginine side chains.

The changes in heat capacity upon mutation are quite small (5 to 13% of $\Delta C_{p,A}$), within the experimental uncertainty (Table 1). It should be considered, however, that the total heat capacity decrement is largely dominated by the refolding of the basic region. Since single alanine mutation are not expected to alter the coil-to-helix transition of the basic region significantly, and the "rigid-body" heat capacity change is rather small (−1 kJ K^{-1} mol^{-1} or smaller), the measured $\Delta\Delta C_{p,A}$ values become sizable. There is no correlation between the experimental $\Delta\Delta C_{p,A}$ and the amount of polar, nonpolar, and total buried surface change caused by mutation. Interestingly, $\Delta\Delta C_{p,A}$ strongly correlates with the free energy effect of the mutations ($\Delta\Delta G_A$). The stabilizing N19A replacement is linked to the largest negative heat capacity increment (−0.4 kJ mol^{-1} K^{-1}), while the most destabilizing mutation (R25A) is accompanied by the largest positive $\Delta\Delta C_{p,A}$ (0.5 kJ mol^{-1} K^{-1}). Overall, $\Delta\Delta C_{p,A}$ and $\Delta\Delta G_A$ are correlated by $R^2 = 0.96$. This observation possibly indicates a complicated balance of forces and mechanisms leading to change in affinity, since neither differential parameter (including $\Delta\Delta H_A$ and $\Delta\Delta S_A$) correlates with the change of surface burial upon mutation, and there are no other cross-correlations between $\Delta\Delta X$ parameters.

For all sites entropic factors disfavor the wild type side chains, or else are negligible. The entropy gain cannot be explained with the gain of side chain entropy when longer side chains are replaced by alanine, since the wild type arginine side chains appear not to be penalized entropically. We note the general trend that the favorable entropic effect

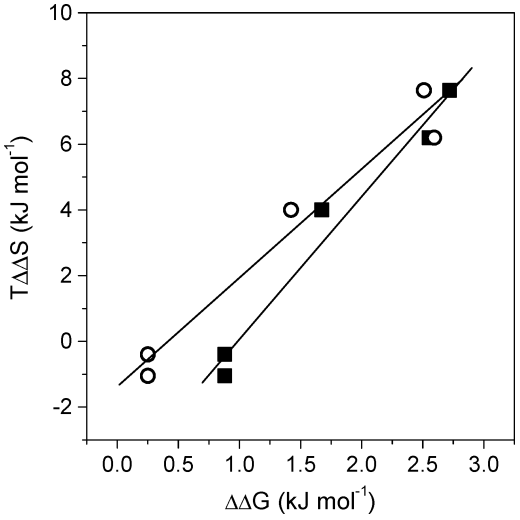

FIGURE 10: Correlation between the measured change in entropy upon X-to-Ala substitutions of side chains in the basic region of Max p21 and the α-helical propensity of the replaced side chains. $T\Delta\Delta S$ is plotted against $\Delta\Delta G$, which ranks the amino acid side chains according to their preference to adopt α-helical conformation (low $\Delta\Delta G$ indicates high α-helix propensity, relative to alanine, for which $\Delta\Delta G = 0$). The helix propensity scales derived entirely from experimental data with peptides and proteins are shown. Filled symbols, scale by Pace and Scholtz ($R^2 = 0.97$; ref (*43*)). Open symbols, scale AGADIR ($R^2 = 0.96$; ref (*44*)).

decreases the closer the site of mutation is to the point where the basic region emerges from helix H1. Sauvé et al. have demonstrated by NMR the existence of a persistent helical turn spanning residues Arg 25 to Ile 29 in the absence of DNA, even at 35 °C (*12*). Furthermore, the Arg 25 and Arg 26 side chains adopt an extended conformation, which is virtually identical to the conformation observed in the Max p21/E-box complex. It is therefore natural to assume that substituting either residue by alanine (having higher, yet very similar helical propensity as arginine) would not interfere with both the fractional population of the helical turn and the conformation of the adjacent arginine side chain. Differently, His 18, Asn 19, Glu 22, and Arg 23 obtain a stable α-helical conformation only in the context of the protein−DNA complex, but may exist in transient α-helical states also in the free protein. As far as stabilization of such states spanning the basic region in the free protein would decrease the entropic penalty for finding the proper conformation facilitating formation of intermolecular contacts, alanine mutation in the corresponding sites is expected to stabilize the complex entropically. Figure 10 illustrates the very strong correlation between the increase in α-helical propensity upon X-to-Ala mutation and the entropic benefit the mutation exhibits. Although alanine substitutions might diminish the entropic penalty, the *total* energetic effect of mutation is greatly modulated by the enthalpic factors (i.e., formation/breakage of bonds and the concomitant hydration changes). This point is nicely illustrated by comparing the energetic signature of H18A and N19A mutations.

The energetic effect of the R50A mutation is balanced in a radically different way. First, both the enthalpy and the entropy changes are much larger than the changes observed for all other sites. Second, the replacement is favored by a large enthalpic effect and is disfavored by an even larger entropic effect. Since the mutation eliminates only one of the two contacts of Arg 50 to the phosphate backbone (the second one being formed by the peptide amide), this means that the interactions formed by the Arg 50 side chain destabilize the wild type complex enthalpically, yet strongly promote DNA binding entropically. Both the magnitude and the sign of the observed energetic changes are very unlikely caused by elimination of a single contact to the phosphate backbone. Rather, we envisage contributions from structural rearrangements of the protein in response to the mutation. The methylene groups of the Arg 50 side chain pack against Ile 29 and Phe 33 and complement the HLH hydrophobic core. These interactions are present both in the X-ray structure of the Max p21-E-box complex and in the NMR ensemble of the free Max protein but are eliminated in the Max $p21^{R50A}$ mutant. Two nonexclusive scenarios are possible. (i) Removal of the hydrophobic moiety of the Arg 50 side chain by alanine mutation causes loosening of the packing of the HLH hydrophobic core and promotes local unfolding. In the Max $p21^{R50A}$/DNA complex, the contact made by the peptide amide to the phosphate backbone facilitates consolidation of the packing interactions in the region. (ii) Alternatively, strong contacts to DNA made simultaneously by the Arg 50 guanidino and amide groups might lead to a "conformational strain" and suboptimal packing of the side chain methylene groups to Ile 29 and Phe 33. If the second contact to DNA is removed by mutation, no structural changes are imposed in the region. It is not possible to distinguish between the two scenarios, yet both are fully compatible with the observed energetic signature of the R50A mutation. Loosening (suboptimal packing) of hydrophobic interactions in the HLH core is linked to disruption of enthalpically rich contacts, but a less tightly packed, and possibly more flexible region will be entropically favored. Also, although the difference is small in magnitude, $\Delta C_{p,A}{}^{R50A}$ is more negative than $\Delta C_{p,A}{}^{WT}$, as expected for a process linked to burial of hydrophobic surface. Not only for this site, a rigorous analysis of the energetic partitioning of the observed changes in affinity arising from structure perturbation is unfortunately hampered by the lack of high-resolution structural information on all relevant states comprising the thermodynamic system.

CONCLUSIONS

We have presented a complete description of the thermodynamic stability of the full length gene product of the Max transcription factor p21 isoform, and an in-depth characterization of the energetics of DNA binding. The combined results provide insights into the mechanistic basis of sequence-specific E-box recognition by proteins of the Myc/Max/Mad family. Direct heat capacity and enthalpy measurements demonstrate that the N- and C-terminal segments flanking the core b-HLH-LZ domain and accounting for half of the protein are disordered, do not participate in packing interactions, and are not involved in DNA binding. Their role in promoting the biological effects of Max is still poorly understood. However, the dissociation constant of Max p21 is in the low micromolar range ($\sim 4 \times 10^{-6}$ M) at 37 °C. At this temperature Max p21 binds the E-box target with affinity in the low nanomolar range. Considering that the nuclear concentration of Max p21 has been estimated to be about micromolar (*9*), the Max homodimeric state is populated and likely binds to E-box targets to affect transcription.

The DNA binding reaction is driven by net favorable enthalpy changes and is opposed by the net entropic changes. The refolding of the unstructured basic region of the free protein to the binding-competent α-helical state significantly contributes to the overall thermodynamic parameters. Stabilization of the LZ subdomain increases the affinity of Max p21 to DNA. The results suggest that thermodynamic coupling between HLH and LZ leads to subtle structural changes, as the consequence of which two Max residues form additional electrostatic contacts with the DNA phosphates, the likely candidates being Lys 30 from helix H1 and Lys 47 from the loop.

We have probed the energetic importance of evolutionary conserved residues that form well-defined contacts to the E-box target DNA bases or backbone phosphates according to X-ray data. Five side chains contribute modestly to binding affinity (15−160× decrease in K_D upon alanine mutation). One notable exception is Arg 26, which confers substantial stabilization. Although in close contact to the phosphate backbone, the Asn 19 side chain appears energetically unimportant. Altogether, the presented data point to the central role of the helical turn encompassing the C-terminus of the basic region and the start of helix H1. The preformed bivalent helical scaffold possibly anchors the protein to DNA at little expense of conformational entropy by positioning the energetically most important Arg 25 and Arg 26 to form three backbone contacts and one base-specific, deeply buried hydrogen bond. Association may be fast and dissociation may be slow since the clustered positive charges of Arg 25, Arg 26, and Arg 50 provide a steering force toward DNA. Furthermore, once stabilized, this conformation might serve as the nucleation site for propagation of α-helix toward the N-terminus of the basic region. Analysis of the thermodynamic signature of alanine mutants suggests that there are pronounced, context-dependent differences in the energetic content of formally identical protein−DNA contacts (for instance arginine−backbone phosphate bonds). Since the degree of sequence conservation in the basic and loop regions of Myc/Mad/Max family members is not absolute, future results from structural and biophysical experiments, and molecular mechanics approaches are required to elucidate the detailed structure−energetics relationships in DNA recognition by b-HLH-LZ proteins.

ACKNOWLEDGMENT

The authors thank Stoyan Milev for initial ITC experiments, Serge Chesnov for mass spectrometry analysis, and Christine Berger-Sprecher for stimulating discussions.

SUPPORTING INFORMATION AVAILABLE

Figures describing AUC analysis of the oligomerization state of Max p21, the influence of the monomer−dimer equilibrium on the shape of the binding isotherms, and analysis of the heat capacities of Max p21, E-box DNA, and the protein−DNA complex. This material is available free of charge via the Internet at http://pubs.acs.org.

REFERENCES

1. Amati, B., and Land, H. (1994) Myc−Max−Mad: a transcription factor network controlling cell cycle progression, differentiation and death, *Curr. Opin. Genet. Dev. 4*, 102−108.
2. Grandori, C., Cowley, S. M., James, L. P., and Eisenman, R. N. (2000) The Myc/Max/Mad network and the transcriptional control of cell behavior, *Annu. Rev. Cell Dev. Biol. 16*, 653−699.
3. Henriksson, M., and Luscher, B. (1996) Proteins of the Myc network: Essential regulators of cell growth and differentiation, *Adv. Cancer Res. 68*, 109−182.
4. Zhou, Z. Q., and Hurlin, P. J. (2001) The interplay between Mad and Myc in proliferation and differentiation, *Trends Cell Biol. 11*, S10−S14.
5. Toyo-oka, K., Bowen, T. J., Hirotsune, S., Li, Z., Jain, S., Ota, S., Lozach, L. E., Bassett, I. G., Lozach, J., Rosenfeld, M. G., Glass, C. K., Eisenman, R. N., Ren, B., Hurlin, P. J., and Wynshaw-Boris, A. (2006) Mnt-Deficient Mammary Glands Exhibit Impaired Involution and Tumors with Characteristics of Myc Overexpression, *Cancer Res. 66*, 5565−5573.
6. Banerjee, A., Hu, J., and Goss, D. J. (2006) Thermodynamics of Protein-Protein Interactions of cMyc, Max, and Mad: Effect of Polyions on Protein Dimerization, *Biochemistry 45*, 2333−2338.
7. Brownlie, P., Ceska, T. A., Lamers, M., Romier, C., Stier, G., Teo, H., and Suck, D. (1997) The crystal structure of an intact human Max-DNA complex: new insights into mechanisms of transcriptional control, *Structure 5*, 509−520.
8. Ferre-D'Amare, A. R., Prendergast, G. C., Ziff, E. B., and Burley, S. K. (1993) Recognition by Max of Its Cognate DNA through a Dimeric B/Hlh/Z Domain, *Nature 363*, 38−45.
9. Nair, S. K., and Burley, S. K. (2003) X-ray structures of Myc-Max and Mad-Max recognizing DNA: Molecular bases of regulation by proto-oncogenic transcription factors, *Cell 112*, 193−205.
10. Anthony-Cahill, S. J., Benfield, P. A., Fairman, R., Wasserman, Z. R., Brenner, S. L., Stafford, W. F., Altenbach, C., Hubbell, W. L., and Degrado, W. F. (1992) Molecular Characterization of Helix-Loop-Helix Peptides, *Science 255*, 979−983.
11. Fisher, D. E., Parent, L. A., and Sharp, P. A. (1993) High-Affinity DNA-Binding Myc Analogs - Recognition by an Alpha-Helix, *Cell 72*, 467−476.
12. Sauve, S., Tremblay, L., and Lavigne, P. (2004) The NMR solution structure of the max b/HLH/LZ free of DNA: Insights into the reversible DNA binding mechanism of dimeric transcription factors, *J. Mol. Biol. 13*, 161−162.
13. Hu, J. Z., Banerjee, A., and Goss, D. J. (2005) Assembly of b/HLH/z proteins c-Myc, Max, and Mad1 with cognate DNA: Importance of protein-protein and protein-DNA interactions, *Biochemistry 44*, 11855−11863.
14. Jung, K. C., Rhee, H. S., Park, C. H., and Yang, C.-H. (2005) Determination of the dissociation constants for recombinant c-Myc, Max, and DNA complexes: The inhibitory effect of linoleic acid on the DNA-binding step, *Biochem. Biophys. Res. Commun. 334*, 269−275.
15. Park, S., Chung, S., Kim, K.-M., Jung, K.-C., Park, C., Hahm, E.-R., and Yang, C.-H. (2004) Determination of binding constant of transcription factor myc-max/max-max and E-box DNA: the effect of inhibitors on the binding, *Biochim. Biophys. Acta 1670*, 217−228.
16. Naud, J., Montagne, M., McDuff, F., Chabot, B., and Lavigne, P. (2005) Structural and thermodynamical analysis of the complete p21 gene product of Max, *Biochemistry 44*, 12746−12758.
17. Naud, J.-F., Gagnon, F., Wellinger, R., Chabot, B., and Lavigne, P. (2003) Improving the Thermodynamic Stability of the Leucine Zipper of Max Increases the Stability of its b-HLH-LZ:E-box complex, *J. Mol. Biol. 326*, 1577−1595.
18. Pace, C. N. (1986) Determination and analysis of urea and guanidine hydrochloride denaturation curves, *Methods Enzymol. 131*, 266−280.
19. Plotnikov, V. V., Brandts, J. M., Lin, L. N., and Brandts, J. F. (1997) A new ultrasensitive scanning calorimeter, *Anal. Biochem. 250*, 237−244.
20. Freire, E. (1995) Thermal denaturation methods in the study of protein folding, *Methods Enzymol. 259*, 144−169.
21. Privalov, P. L., and Potekhin, S. A. (1986) Scanning microcalorimetry in studying temperature-induced changes in proteins, *Method Enzymol 131*, 4−51.
22. Wiseman, T., Williston, S., Brandts, J. F., and Lin, L. N. (1989) Rapid Measurement of Binding Constants and Heats of Binding Using a New Titration Calorimeter, *Anal. Biochem. 179*, 131−137.
23. Ferre-D'Amare, A. R., and Burley, S. K. (1994) Use of Dynamic Light-Scattering to Assess Crystallizability of Macromolecules and Macromolecular Assemblies, *Structure 2*, 567−567.

24. Manning, G. S. (1978) The molecular theory of polyelectrolyte solutions with applications to the electrostatic properties of polynucleotides, *Q. Rev. Biophys. 11*, 179−246.
25. Record, M. T., Jr., Ha, J. H., and Fisher, M. A. (1991) Analysis of equilibrium and kinetic measurements to determine thermodynamic origins of stability and specificity and mechanism of formation of site-specific complexes between proteins and helical DNA, *Methods Enzymol. 208*, 291−343.
26. Plotnikov, V., Rochalski, A., Brandts, M., Brandts, J. F., Williston, S., Trasca, V., and Lin, L.-N. (2002) An autosampling differential scanning calorimeter instrument for studying molecular interactions, *ASSAY Drug Dev. Technol. 1*, 83−90.
27. Richardson, J. M., Lopez, M. M., and Makhatadze, G. I. (2005) Enthalpy of helix-coil transition: Missing link in rationalizing the thermodynamics of helix-forming propensities of the amino acid residues, *Proc. Natl. Acad. Sci. U.S.A. 102*, 1413−1418.
28. Rose, G. D., Fleming, P. J., Banavar, J. R., and Maritan, A. (2006) A backbone-based theory of protein folding, *Proc. Natl. Acad. Sci. U.S.A. 103*, 16623−16633.
29. Dragan, A. I., Frank, L., Liu, Y. Y., Makeyeva, E. N., Crane-Robinson, C., and Privalov, P. L. (2004) Thermodynamic signature of GCN4-bZIP binding to DNA indicates the role of water in discriminating between the AP-1 and ATF/CREB sites, *J. Mol. Biol. 343*, 865−878.
30. Doig, A. J., and Sternberg, M. J. E. (1995) Side-Chain Conformational Entropy in Protein-Folding, *Protein Sci. 4*, 2247−2251.
31. D'Aquino, J. A., Gomez, J., Hilser, V. J., Lee, K. H., Amzel, L. M., and Freire, E. (1996) The magnitude of the backbone conformational entropy change in protein folding, *Proteins 25*, 143−156.
32. Luque, I., and Freire, E. (1998) Structure-based prediction of binding affinities and molecular design of peptide ligands, *Method Enzymol. 295*, 100−127.
33. Baker, B. M., and Murphy, K. P. (1997) Dissecting the energetics of a protein-protein interaction: the binding of ovomucoid third domain to elastase, *J. Mol. Biol. 268*, 557−569.
34. Milev, S., Gorfe, A. A., Karshikoff, A., Clubb, R. T., Bosshard, H. R., and Jelesarov, I. (2003) Energetics of sequence-specific Protein-DNA association: Binding of integrase Tn916 to its target DNA, *Biochemistry 42*, 3481−3491.
35. Privalov, P. L., Jelesarov, I., Read, C. M., Dragan, A. I., and Crane-Robinson, C. (1999) The energetics of HMG box interactions with DNA: Thermodynamics of the DNA binding of the HMG box from mouse Sox-5, *J. Mol. Biol. 294*, 997−1013.
36. Olmsted, M. C., Bond, J. P., Anderson, C. F., and Record, M. T., Jr. (1995) Grand canonical Monte Carlo molecular and thermodynamic predictions of ion effects on binding of an oligocation (L8+) to the center of DNA oligomers, *Biophys. J. 68*, 634−647.
37. Bird, G. H., Lajmi, A. R., and Shin, J. A. (2002) Sequence-specific recognition of DNA by hydrophobic, alanine-rich mutants of the basic region/leucine zipper motif investigated by fluorescence anisotropy, *Biopolymers 65*, 10−20.
38. Park, S., Boder, E. T., and Saven, J. G. (2005) Modulating the DNA affinity of Elk-1 with computationally selected mutations, *J. Mol. Biol. 348*, 75−83.
39. Fisher, F., and Goding, C. R. (1992) Single Amino-Acid Substitutions Alter Helix Loop Helix Protein Specificity for Bases Flanking the Core Canntg Motif, *EMBO J. 11*, 4103−4109.
40. Dang, C. V., Dolde, C., Gillison, M. L., and Kato, G. J. (1992) Discrimination between Related DNA Sites by a Single Amino-Acid Residue of Myc-Related Basic Helix Loop Helix Proteins, *Proc. Natl. Acad. Sci. U.S.A. 89*, 599−602.
41. Sauve, S., Naud, J.-F., and Lavigne, P. (2007) The Mechanism of Discrimination between Cognate and Non-Specific DNA by Dimeric b/HLH/LZ Transcription Factors, *J. Mol. Biol. 365*, 1163−1175.
42. Griffith, K. L., and Wolf, J. R. E. (2002) A Comprehensive Alanine Scanning Mutagenesis of the Escherichia coli Transcriptional Activator SoxS: Identifying Amino Acids Important for DNA Binding and Transcription Activation, *J. Mol. Biol. 322*, 237−257.
43. Pace, C. N., and Scholtz, J. M. (1998) A Helix Propensity Scale Based on Experimental Studies of Peptides and Proteins. *Biophys. J. 75*, 422−427.
44. Lacroix, E., and Viguera, A. R., & Serrano, L. (1998) Elucidating the folding problem of [alpha]-helices: local motifs, long-range electrostatics, ionic-strength dependence and prediction of NMR parameters. *J. Mol. Biol. 284*, 173−191.

BI701081Q